LETTER

doi:10.1038/nature11776

# Reciprocal regulation of p53 and malic enzymes modulates metabolism and senescence

Peng Jiang[1]*, Wenjing Du[1]*, Anthony Mancuso[1], Kathryn E. Wellen[1] & Xiaolu Yang[1]

**Cellular senescence both protects multicellular organisms from cancer and contributes to their ageing[1]. The pre-eminent tumour suppressor p53 has an important role in the induction and maintenance of senescence, but how it carries out this function remains poorly understood[1–3]. In addition, although increasing evidence supports the idea that metabolic changes underlie many cell-fate decisions and p53-mediated tumour suppression, few connections between metabolic enzymes and senescence have been established. Here we describe a new mechanism by which p53 links these functions. We show that p53 represses the expression of the tricarboxylic-acid-cycle-associated malic enzymes ME1 and ME2 in human and mouse cells. Both malic enzymes are important for NADPH production, lipogenesis and glutamine metabolism, but ME2 has a more profound effect. Through the inhibition of malic enzymes, p53 regulates cell metabolism and proliferation. Downregulation of ME1 and ME2 reciprocally activates p53 through distinct MDM2- and AMP-activated protein kinase-mediated mechanisms in a feed-forward manner, bolstering this pathway and enhancing p53 activation. Downregulation of ME1 and ME2 also modulates the outcome of p53 activation, leading to strong induction of senescence, but not apoptosis, whereas enforced expression of either malic enzyme suppresses senescence. Our findings define physiological functions of malic enzymes, demonstrate a positive-feedback mechanism that sustains p53 activation, and reveal a connection between metabolism and senescence mediated by p53.**

We previously found that p53 inhibits the important NADPH producer glucose-6-phosphate dehydrogenase[4]. As this did not fully explain the effect of p53 on NADPH, we investigated whether p53 controls the expression of malic enzymes, which catalyse the oxidative decarboxylation of malate to generate pyruvate and either NADPH or NADH[5,6] (Supplementary Fig. 1). In mammalian cells, three malic enzyme isoforms have been identified: a cytosolic $NADP^+$-dependent isoform (ME1), a mitochondrial $NAD(P)^+$-dependent isoform (ME2) and a mitochondrial $NADP^+$-dependent isoform (ME3), of which ME1 and ME2 are the main isoforms (Supplementary Fig. 2a)[7]. By recycling the tricarboxylic acid (TCA) cycle intermediate malate into the common TCA cycle carbon source pyruvate, malic enzymes may have a regulatory role in matching TCA flux to cellular demand for energy, reducing equivalents and biosynthetic precursors (Supplementary Fig. 1).

We knocked down *TP53* in human osteosarcoma U2OS cells and normal diploid fibroblast IMR90 cells using short hairpin RNA (shRNA). This led to a significant increase in messenger RNA levels of *ME1* and *ME2* (Fig. 1a, b and Supplementary Fig. 2b), accompanied by increased protein levels and total enzymatic activity of ME1 and ME2 (Fig. 1a, c and Supplementary Fig. 2c). Likewise, expression of ME1 and ME2 were substantially higher in *Trp53* knockout ($Trp53^{-/-}$) compared to p53-wild-type ($Trp53^{+/+}$) mouse embryonic fibroblasts (MEFs) (Fig. 1d). The normally short-lived p53 protein is stabilized by DNA-damage signals. Cells treated with the genotoxic agents etoposide and doxorubicin showed both time- and concentration-dependent reductions in the expression of ME1 and ME2 (Fig. 1e and Supplementary Fig. 2b, d–g). When *TP53* was knocked down, the expression of ME1 and ME2 no longer responded to DNA damage (Fig. 1e). These results indicate that the expression of ME1 and ME2 is controlled by p53, both at basal levels and when p53 is stabilized by DNA-damage signals.

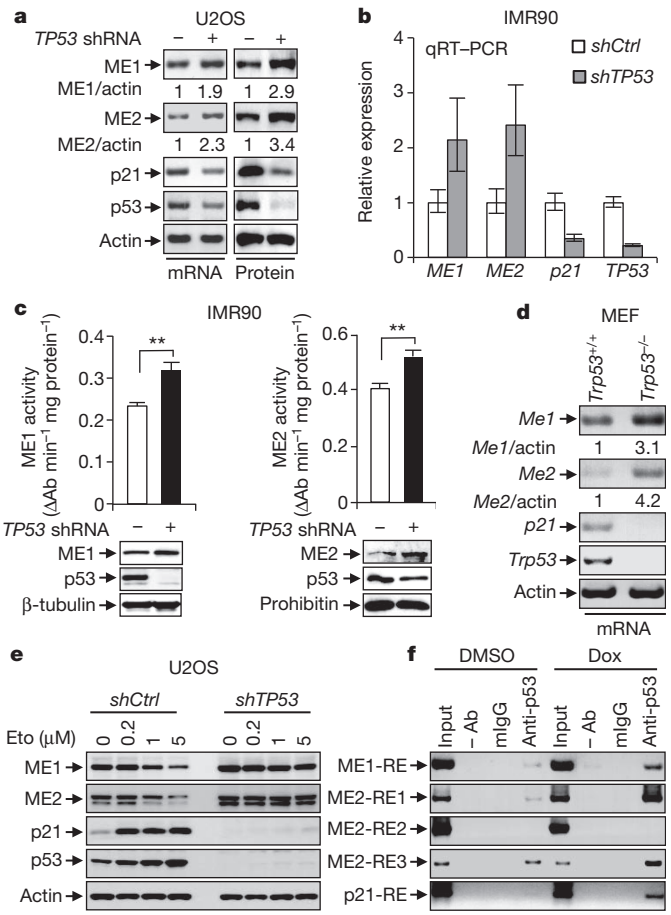


**Figure 1 | p53 represses the expression of malic enzymes.** **a**, Malic enzyme mRNA and protein expression in U2OS cells stably expressing *TP53* shRNA or control (Ctrl) shRNA. Relative malic enzyme/actin ratios are given. **b**, **c**, mRNA expression (**b**), total activity and protein levels (**c**) of malic enzymes in *TP53*-depleted and control IMR90 cells. Data shown are mean ± s.d. ($n = 3$). **d**, Malic enzyme gene expression in $Trp53^{+/+}$ and $Trp53^{-/-}$ MEFs. **e**, *TP53*-depleted and control U2OS cells were treated with increasing amounts of etoposide (Eto) and assayed for malic enzyme expression. **f**, $TP53^{+/+}$ HCT116 cells treated with or without doxorubicin (Dox; 1 μg $ml^{-1}$) were subjected to chromatin immunoprecipitation assay with anti-p53 DO-1 antibody, control mouse IgG (mIgG), or no antibody (− Ab). DMSO, dimethylsulphoxide; qRT–PCR, quantitative reverse-transcriptase PCR. $^{**}P < 0.01$.

[1]Department of Cancer Biology and Abramson Family Cancer Research Institute, University of Pennsylvania School of Medicine, Philadelphia, Pennsylvania 19104, USA.
*These authors contributed equally to this work.

By analysing the malic enzyme gene sequences, we identified a putative p53 response element[8] in the first intron of the *ME1* gene (ME1-RE) and three putative response elements in the first intron of the *ME2* gene (ME2-RE1, ME2-RE2 and ME2-RE3) (Supplementary Fig. 3a). Chromatin immunoprecipitation assays in HCT116 cells revealed that p53 bound to the genomic regions of ME1-RE, ME2-RE1 and ME2-RE3, but not ME2-RE2. This binding was further enhanced when p53 was stabilized by treatment with doxorubicin (Fig. 1f). In addition, p53 repressed the expression of a luciferase gene driven by the genomic fragment containing ME1-RE, ME2-RE1 or ME2-RE3, but not ME2-RE2 (Supplementary Fig. 3b). p53-mediated repression of certain target genes involves histone deacetylases[9]. Treatment with trichostatin A, an inhibitor of histone deacetylases, abrogated p53-mediated repression of *ME1* and *ME2* genes (Supplementary Fig. 2g).

*TP53* deficiency also led to a strong increase in the *ME3* transcript (Supplementary Fig. 4a). A putative p53 response element is present in the first intron of the *ME3* gene (ME3-RE) (Supplementary Fig. 4b). p53 bound to the genomic region of ME3-RE in cells (Supplementary Fig. 4c) and reduced the expression of a luciferase reporter driven by this response element (Supplementary Fig. 4d). Given the low abundance of ME3 expression in cell lines that have been tested (Supplementary Fig. 2a)[7], we focused on ME1 and ME2 in subsequent analyses.

Although ME1 and ME2 have been extensively characterized *in vitro*, there is a paucity of information on their functions in cells. Silencing *ME1* and *ME2*—in particular *ME2*—with short interfering RNA (siRNA) reduced cellular NADPH levels in IMR90 and U2OS cells (Fig. 2a and Supplementary Fig. 5a). This effect was also observed when a separate set of malic enzyme siRNAs, as well as malic enzyme shRNAs, were used (Supplementary Fig. 5b, c). By contrast, forced expression of ME1 or ME2—in particular ME2—or the addition of a malic enzyme substrate (dimethyl L-malate) increased cellular NADPH levels (Fig. 2b lanes 1–3, and Supplementary Fig. 5d). To determine whether the effect of malic enzymes is due to their enzymatic activity, we generated two ME1 mutations ($ME1^{mut1}$ and $ME1^{mut2}$) and three ME2 mutations ($ME2^{mut1}$, $ME2^{mut2}$ and $ME2^{mut3}$), each of which exhibited little or no enzymatic activity *in vitro* as well as *in vivo* (Supplementary Fig. 6). None of these mutants were able to increase cellular NADPH levels (Fig. 2b, lanes 4–10). Thus, both ME1 and ME2 are required for maintaining cellular NADPH levels through their enzymatic activity, with ME2 having a more profound effect. As previously observed[4], knockdown of *TP53* led to a significant increase in NADPH levels. This increase was partially reversed through the silencing of *ME1* and near-completely reversed through the silencing of *ME2* (Fig. 2a and Supplementary Fig. 5a, b). These results indicate that p53 regulates NADPH metabolism through the suppression of both malic enzymes, particularly ME2.

As NADPH provides reducing equivalents for reductive biosynthesis, we examined the role of malic enzymes in lipid production. MEF cells and murine-derived 3T3-L1 pre-adipocytes were cultured with a cocktail that stimulated their differentiation into adipocytes[4,10]. Triglycerides and total lipid levels in these cells declined when *Me1* or *Me2*—particularly *Me2*—was depleted in these cells (Fig. 2c and Supplementary Fig. 7). By contrast, overexpression of both enzymes, particularly ME2, but none of the ME1 or ME2 mutants, increased lipid abundance (Fig. 2d). Concordant with previously published data[4], we observed a marked increase in lipid levels in *Trp53*-deficient cells compared to *Trp53*-proficient cells. *Me1* knockdown partially reversed this increase, whereas *Me2* knockdown prevented it entirely, correlating with its greater influence on cellular NADPH levels (Fig. 2c and Supplementary Fig. 7). These results indicate that the enhanced lipid accumulation in p53-deficient cells is dependent on the malic enzymes, especially ME2.

Silencing of *ME2*, as well as of *ME1*, did not significantly alter NADH levels or the $NAD^+$/NADH ratio in IMR90 cells (Supplementary Fig. 8a, b), despite the fact that ME2 is characterized as either $NADP^+$ or $NAD^+$ dependent[5,6]. NADH is the main electron donor for the electron transport chain that drives ATP production. Silencing of either malic enzyme did not significantly alter the abundance of cellular ATP or ADP in IMR90 cells (Supplementary Fig. 8c). In U2OS cells silencing of *ME1*, but not *ME2*, reduced NADH levels and increased the $NAD^+$/NADH ratio (Supplementary Fig. 8d, e). These results are consistent with a cell-type-specific role of ME1 and a minimal role of ME2 in maintaining cellular NADH and ATP levels.

Next we investigated the role of ME1 and ME2 in the metabolism of glucose and glutamine. In $TP53^{-/-}$ HCT116 cells silencing of either malic enzyme, but especially *ME2*, strongly reduced glutamine

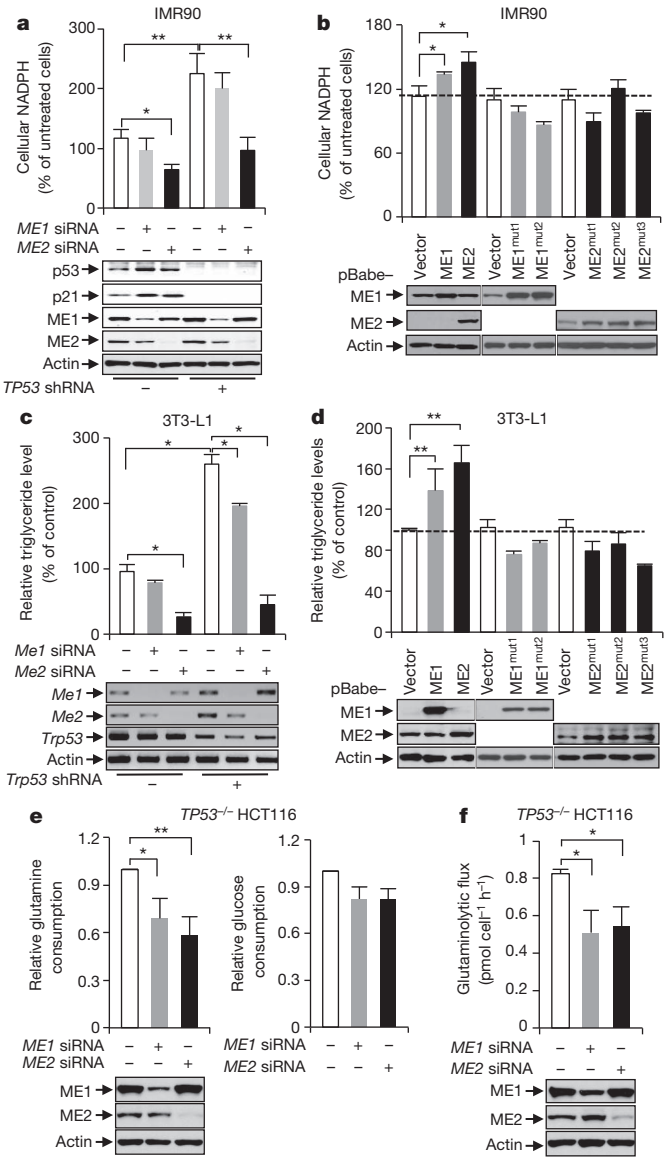


**Figure 2 | ME1 and ME2 influence NADPH production, lipid production and glutaminolysis.** **a**, **b**, NADPH levels in *TP53*-depleted and control IMR90 cells transfected with control, *ME1* or *ME2* siRNA (**a**), or in IMR90 cells stably overexpressing wild-type malic enzymes, mutant malic enzymes or vector control (**b**). Protein expression is shown below. Stable protein expression was achieved using the pBabe retroviral expression system. **c**, **d**, Triglyceride contents in *Trp53*-depleted and control 3T3-L1 cells transfected with control, *Me1* or *Me2* siRNA (**c**), or 3T3-L1 cells stably expressing wild-type malic enzymes, mutant malic enzymes or vector control (**d**). mRNA (**c**) and protein (**d**) expression is shown below. **e**, **f**, Effect of *ME1* and *ME2* knockdown in $TP53^{-/-}$ HCT116 cells on glucose and glutamine consumption (**e**) and glutaminolytic flux (**f**). Protein expression is shown below. All error bars represent mean ± s.d. ($n = 3$). $^*P < 0.05$; $^{**}P < 0.01$.

consumption (Fig. 2e), whereas silencing of either malic enzyme had a moderate effect on glucose consumption. We extended this analysis by evaluating the rate of glutaminolysis. Depletion of either *ME1* or *ME2* noticeably slowed down glutaminolytic flux (Fig. 2f). These results indicate that both ME1 and ME2 have a key role in glutamine metabolism but a relatively minor role in glucose metabolism.

p53 is critical for the induction and maintenance of senescence[1–3]. We noticed that in IMR90 cells, a well-established senescence model, silencing of each malic enzyme by either siRNA or shRNA caused a profound increase in cells expressing senescence-associated β-galactosidase, stopping growth (Fig. 3a, b and Supplementary Fig. 9a–f). The induction of senescence in malic-enzyme-knockdown cells was also indicated by the marked accumulation the promyelocytic leukaemia protein nuclear bodies[11,12] (Fig. 3c and Supplementary Fig. 9g). Notably, even a moderate reduction (20–30%) in either *ME1* or *ME2* strongly elicited senescence (Supplementary Fig. 10a). Malic-enzyme-loss-induced senescence also occurred in U2OS and *TP53*$^{+/+}$ HCT116 tumour cell lines (Supplementary Fig. 10b, c). In *TP53*-deficient primary and tumour cell lines senescence decreased markedly and malic enzyme depletion lost its ability to induce this phenotype (Fig. 3b, c and Supplementary Figs 9b, c, f, g and 10c). By contrast, malic enzyme depletion did not cause cell death (Supplementary Fig. 11a); it induced the expression of p53 target genes implicated in senescence[2,13] but not apoptosis (Supplementary Fig. 11b). These data indicate that downregulation of malic enzymes induces senescence through p53.

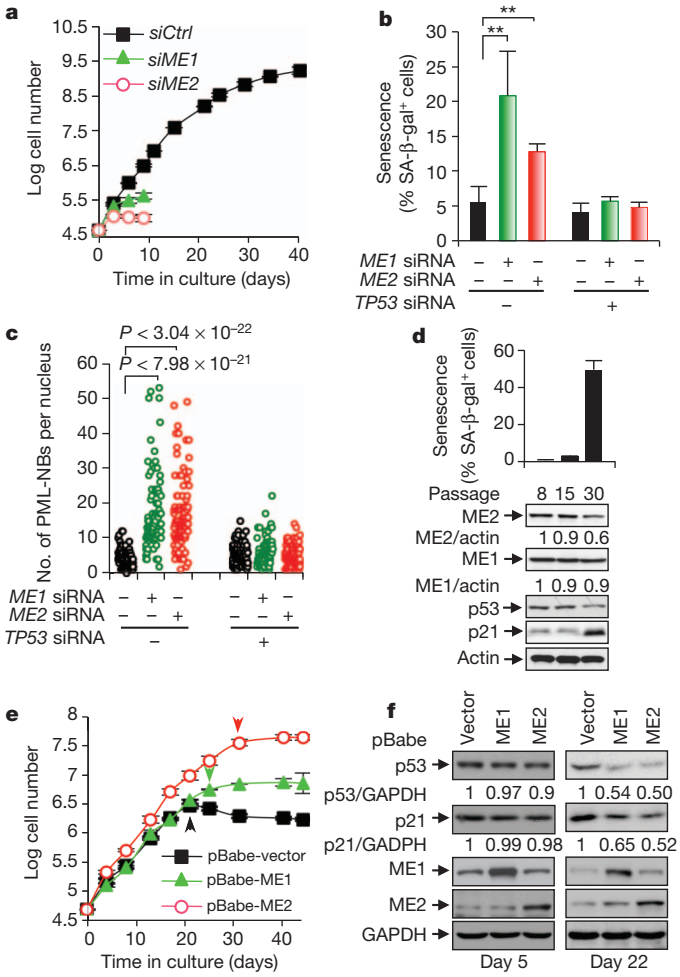


**Figure 3 | A role for malic enzymes in suppressing p53-mediated senescence.** **a**, The replicative lifespan of IMR90 cells transfected with control, *ME1* or *ME2* siRNA. **b**, **c**, IMR90 cells transfected with *ME1*, *ME2*, *TP53* or control siRNA as indicated. Percentages of senescence-associated β-galactosidase (SA-β-gal)-positive cells (**b**) and numbers of promyelocytic leukaemia nuclear bodies (PML-NBs) (**c**) are shown (see Supplementary Fig. 9f, g for representative images). **d**, Percentages of SA-β-gal-positive cells (top) and protein expression (bottom) in IMR90 cells at different passages. **e**, **f**, Replicative lifespan (**e**) and protein expression (**f**) of IMR90 cells with and without overexpression of ME1 or ME2. Arrows in **e** indicate the onset of senescence. All error bars represent mean ± s.d. ($n = 3$). $^{**}P < 0.01$.

We next examined the role of malic enzymes in replicative senescence of normal human cells, a p53-regulated process[1,3]. IMR90 cells were serially passaged in culture until a substantial number of them (~50%) entered senescence. The expression of ME1 remained at comparable levels at different passages, whereas the expression of ME2, which stayed unchanged initially, noticeably declined at the late stage (Fig. 3d). To test whether the decline in ME2 contributes to senescence in this setting, we evaluated the replicative capacity of IMR90 cells forced to express ME2. Compared with control cells, ME2-overexpressing cells could be cultured for extended passages with a greatly delayed onset of senescence (Fig. 3e and Supplementary Fig. 12a). As ME1 expression was maintained during replicative senescence, we were surprised to observe a delay in senescence when ME1 expression was forced (Fig. 3e and Supplementary Fig. 12a). By contrast, forced expression of any of the malic enzyme mutants did not delay senescence and instead moderately promoted senescence (Supplementary Fig. 12b–d), possibly through a dominant-negative effect on the endogenous malic enzymes. These results indicate that both enzymes—particularly ME2—are capable of suppressing senescence and suggest that the decline in ME2 may contribute to replicative senescence.

To examine the effect of malic enzymes on other scenarios of p53-regulated senescence, we found that culturing IMR90 cells in medium containing no or low levels of glutamine resulted in p53-dependent senescence (Supplementary Fig. 13a, b). This senescence could be delayed by overexpression of either ME1 or ME2 (Supplementary Fig. 13b), or the addition of the malic enzyme substrate malate (Supplementary Fig. 13c). By contrast, exogenous malic enzyme expression did not influence premature senescence of IMR90 cells induced by the oncogene *HrasV12* (Supplementary Fig. 13d), which is not dependent on p53 (refs 14, 15). These results indicate that ME1 and ME2 expression suppress the specific way in which p53 induces senescence.

We investigated the mechanism for senescence induced by malic enzyme downregulation. In IMR90 and U2OS cells in which the expression of either *ME1* or *ME2* was silenced by siRNA, even moderately, p53 levels were increased, accompanied by enhanced phosphorylation of p53 and induction of its target gene *p21* (also known as *CDKN1A*) (Figs 2a and 4a and Supplementary Figs 5a, b and 10a). By contrast, overexpression of ME1 or ME2 in IMR90 cells substantially reduced p53 levels and activity in late passages (Fig. 3f). Overexpression of ME1 or ME2 in U2OS cells also diminished DNA-damage-induced p53 activation (Supplementary Fig. 14). These observations suggest a strong role for malic enzymes in the suppression of p53. They also indicate the existence of a positive-feedback loop for the p53–malic enzyme pathway: a higher p53 level leads to less malic enzyme expression, which alleviates the inhibition of malic enzymes on p53, leading to even higher p53 activation.

We next examined the mechanism for the regulation of p53 by ME1 and ME2. In unstressed cells, MDM2-mediated ubiquitination maintains a low basal level of p53 (ref. 2). When *ME1* was knocked down in both IMR90 and U2OS cells, the abundance of the MDM2 protein and mRNA declined markedly (Fig. 4a and Supplementary Fig. 15a, b), suggesting that ME1 downregulation activates p53 through a reduction in MDM2 expression. *ME2* knockdown did not significantly affect MDM2 levels. Instead, it turned on AMP-activated protein kinase (AMPK) (Fig. 4a and Supplementary Fig. 15a, b), an intracellular energy gauge that activates p53 through phosphorylation[16]. We tested whether AMPK is required for induction of p53 by ME2 by knocking it down in IMR90 and U2OS cells, and by comparing *AMPK* null and wild-type MEFs. In both situations, loss of AMPK expression prevented *ME2* knockdown from activating p53 (Fig. 4b and Supplementary Fig. 15c). Because silencing of *ME2* did not influence

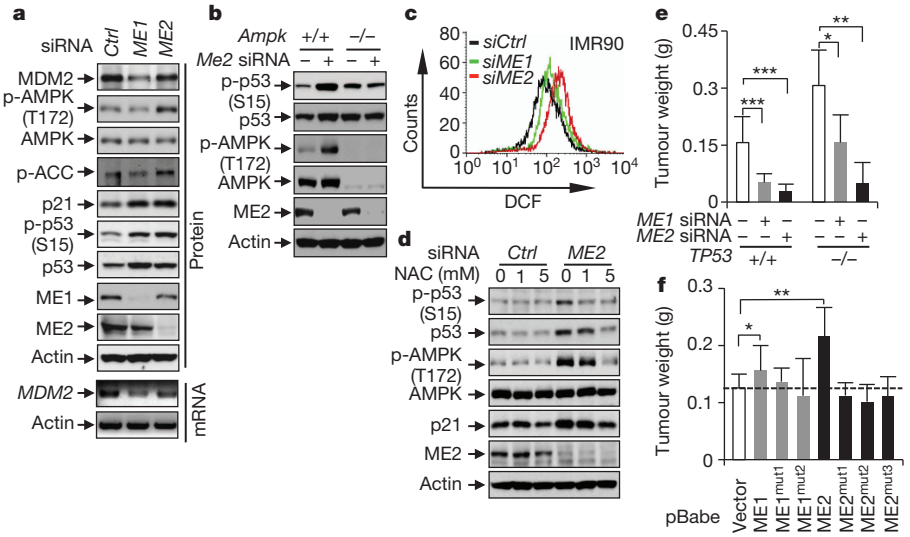


**Figure 4 | Mechanisms of p53 activation induced by malic enzyme downregulation and a role of malic enzymes in tumour growth.** **a**, Effect of *ME1* and *ME2* knockdown on p53 and AMPK activation and MDM2 expression. ACC, acetyl-CoA carboxylase; p-, phosphorylated. **b**, p53 and AMPK activation in $Ampk^{+/+}$ and $Ampk^{-/-}$ MEF cells transfected with control or *Me2* siRNA. **c**, ROS levels, determined by 2′,7′-dichlorodihydrofluorescein diacetate (DCF), in IMR90 cells transfected with *ME1*, *ME2* or control siRNA. **d**, Effect of *N*-acetyl-L-cysteine (NAC) on AMPK and p53 activation in IMR90 cells transfected with control or *ME2* siRNA. **e**, **f**, Average weights of xenograft tumours (mean ± s.d., $n = 6$) generated by $TP53^{+/+}$ and $TP53^{-/-}$ HCT116 cells transfected with *ME1*, *ME2* or control siRNA (**e**), or $TP53^{+/+}$ HCT116 cells stably overexpressing wild-type or mutant malic enzymes (**f**). $*P < 0.05$; $**P < 0.01$; $***P < 0.001$.

cellular ATP levels (Supplementary Fig. 8c), we examined other pathways that could activate AMPK and observed a strong increase in reactive oxygen species (ROS) in various *ME2*-depleted cells (Fig. 4c and Supplementary Fig. 16), correlating with a strong reduction in NADPH levels (Fig. 2a and Supplementary Fig. 5a–c). ROS are a known activator of AMPK[17]. Treatment with the ROS scavenger *N*-acetyl-L-cysteine blocked AMPK and p53 activation (Fig. 4d and Supplementary Fig. 17a, b), abrogated senescence and restored growth of *ME2*-knockdown cells (Supplementary Fig. 17c, d). These results indicate that downregulation of *ME2* increases ROS levels leading to sequential activation of AMPK and p53 and the induction of senescence. In comparison, depletion of *ME1* increased ROS levels moderately in IMR90 cells and minimally in U2OS cells (Fig. 4c and Supplementary Fig. 16), and *N*-acetyl-L-cysteine only slightly affected p53 activation, senescence and growth arrest in *ME1*-depeleted cells (Supplementary Fig. 17b–d).

Previous studies on limited tumour samples suggest that the activity of ME2 is highly increased in these tumours and correlates with tumour progression[18–20]. A survey of public gene-expression databases (http://www.oncomine.org) showed that both ME1 and ME2 expression was significantly upregulated in a variety of human cancers (Supplementary Fig. 18). We investigated whether malic enzymes could influence tumour cell growth. Depletion of *ME1* or *ME2* in U2OS and HCT116 cells, regardless of p53 status, strongly impaired their growth (Supplementary Fig. 19), and reduced the number of cells at the S phase of the cell cycle (Supplementary Fig. 20). By contrast, overexpression of ME1 or ME2, but none of the malic enzyme mutants, enhanced tumour cell growth (Supplementary Fig. 21). In a soft agar assay, tumour cells deprived of malic enzyme gene expression, unlike their control counterparts, failed to form anchorage-independent colonies (Supplementary Fig. 22a, b), whereas cells transduced with wild-type malic enzymes, but not any of the mutants, showed enhanced anchorage-independent growth (Supplementary Fig. 22c, d).

To analyse the function of malic enzymes in the tumour xenograft model, we injected immunocompromised mice with $TP53^{+/+}$ and $TP53^{-/-}$ HCT116 cells treated with *ME1*, *ME2* or control siRNA. $TP53^{-/-}$ HCT116 cells gave rise to tumours that were twice the weight of tumours generated by $TP53^{+/+}$ HCT116 cells. When *ME1* or *ME2*—particularly *ME2*—was silenced in these cells, the tumour sizes were markedly reduced (Fig. 4e and Supplementary Fig. 23a, b). $TP53^{+/+}$ HCT116 tumours devoid of malic enzymes showed extensive senescence and were substantially smaller compared to the corresponding $TP53^{-/-}$ HCT116 tumours (Supplementary Fig. 23c). Conversely, overexpression of wild-type ME1 or ME2, not mutant malic enzymes, accelerated the growth of $TP53^{+/+}$ HCT116 tumours (Fig. 4f and Supplementary Fig. 23d). These observations indicate that malic enzymes are essential for tumour growth through both p53-dependent and -independent mechanisms.

Although p53 is able to induce a range of anti-proliferative responses, emerging evidence indicates that senescence induction and metabolic regulation are central to its function as a tumour suppressor[13,21–25]. Our results demonstrate a positive-feedback loop comprising p53 and malic enzymes that influences p53 activation and links metabolism with the onset of senescence (Supplementary Fig. 24). p53 suppresses all malic enzyme (1, 2 and 3) expression by directly binding to response elements within these genes. Together with our recent finding that p53 targets the NADPH producer glucose-6-phosphate dehydrogenase through a distinct direct catalytic mechanism[4], the current study reveals p53 as a master immediate regulator of cellular NADPH levels. p53 is reciprocally regulated by ME1 and ME2. The marked stabilization of p53 upon *ME1* and *ME2* downregulation is achieved through different mechanisms, through the decline of MDM2 levels and ROS-induced AMPK activation, respectively. These findings support the notion that p53 is a central sentinel for metabolic stresses and coordinates metabolic pathways with cell-fate decision.

Mutual regulation of p53 and malic enzymes is likely a key mechanism that modulates cellular senescence in both normal and tumour cells. Even moderate downregulation of either *ME1* or *ME2* strongly induces p53 activation and senescence, whereas overexpression of either enzyme delays these processes. Thus, these enzymes modulate not only the amplitude, but also the outcome, of p53 activation. p53 is subjected to negative-feedback regulation (for example, the p53–MDM2 feedback loop) that restrains its activity[2]. The p53–malic enzyme positive-feedback loop is likely important to alleviate the negative-feedback regulation so that p53 can accumulate to high levels. This may be particularly relevant in situations in which robust and persistent p53 activation is desirable, such as the induction and maintenance

of senescence. The involvement of the p53–malic enzyme pathway in senescence demonstrates a close link between metabolism and this irreversible fate of the cell.

## METHODS SUMMARY

Malic-enzyme-dependent glutaminolytic flux was determined by labelling the malate pool with $^{13}C$ from [U-$^{13}C_5$]glutamine and monitoring the conversion of [$^{13}C$]malate to pyruvate. $^{13}C$ enrichments were determined with gas chromatography–mass spectrometry. Glucose and glutamine consumption was determined using a YSI 7100 Multiparameter Bioanalytical System. Detailed experimental procedures are presented in Methods.

**Full Methods** and any associated references are available in the online version of the paper.

**Received 5 February; accepted 9 November 2012.**
**Published online 13 January 2013.**

1. Campisi, J. & d'Adda di Fagagna, F. Cellular senescence: when bad things happen to good cells. *Nature Rev. Mol. Cell Biol.* **8,** 729–740 (2007).
2. Vousden, K. H. & Prives, C. Blinded by the light: the growing complexity of p53. *Cell* **137,** 413–431 (2009).
3. Ben-Porath, I. & Weinberg, R. A. The signals and pathways activating cellular senescence. *Int. J. Biochem. Cell Biol.* **37,** 961–976 (2005).
4. Jiang, P. *et al.* p53 regulates biosynthesis through direct inactivation of glucose-6-phosphate dehydrogenase. *Nature Cell Biol.* **13,** 310–316 (2011).
5. Hsu, R. Y. Pigeon liver malic enzyme. *Mol. Cell. Biochem.* **43,** 3–26 (1982).
6. Chang, G. G. & Tong, L. Structure and function of malic enzymes, a new class of oxidative decarboxylases. *Biochemistry* **42,** 12721–12733 (2003).
7. Pongratz, R. L., Kibbey, R. G., Shulman, G. I. & Cline, G. W. Cytosolic and mitochondrial malic enzyme isoforms differentially control insulin secretion. *J. Biol. Chem.* **282,** 200–207 (2007).
8. Riley, T., Sontag, E., Chen, P. & Levine, A. Transcriptional control of human p53-regulated genes. *Nature Rev. Mol. Cell Biol.* **9,** 402–412 (2008).
9. Murphy, M. *et al.* Transcriptional repression by wild-type p53 utilizes histone deacetylases, mediated by interaction with mSin3a. *Genes Dev.* **13,** 2490–2501 (1999).
10. Wellen, K. E. *et al.* ATP-citrate lyase links cellular metabolism to histone acetylation. *Science* **324,** 1076–1080 (2009).
11. Ferbeyre, G. *et al.* PML is induced by oncogenic *ras* and promotes premature senescence. *Genes Dev.* **14,** 2015–2027 (2000).
12. Pearson, M. *et al.* PML regulates p53 acetylation and premature senescence induced by oncogenic Ras. *Nature* **406,** 207–210 (2000).
13. Brady, C. A. *et al.* Distinct p53 transcriptional programs dictate acute DNA-damage responses and tumor suppression. *Cell* **145,** 571–583 (2011).
14. Serrano, M., Lin, A. W., McCurrach, M. E., Beach, D. & Lowe, S. W. Oncogenic *ras* provokes premature cell senescence associated with accumulation of p53 and p16$^{INK4a}$. *Cell* **88,** 593–602 (1997).
15. Wei, W., Hemmer, R. M. & Sedivy, J. M. Role of p14$^{ARF}$ in replicative and induced senescence of human fibroblasts. *Mol. Cell. Biol.* **21,** 6748–6757 (2001).
16. Jones, R. G. *et al.* AMP-activated protein kinase induces a p53-dependent metabolic checkpoint. *Mol. Cell* **18,** 283–293 (2005).
17. Blättler, S. M., Rencurel, F., Kaufmann, M. R. & Meyer, U. A. In the regulation of cytochrome P450 genes, phenobarbital targets LKB1 for necessary activation of AMP-activated protein kinase. *Proc. Natl Acad. Sci. USA* **104,** 1045–1050 (2007).
18. Wasilenko, W. J. & Marchok, A. C. Malic enzyme and malate dehydrogenase activities in rat tracheal epithelial cells during the progression of neoplasia. *Cancer Lett.* **28,** 35–42 (1985).
19. Sauer, L. A., Dauchy, R. T., Nagel, W. O. & Morris, H. P. Mitochondrial malic enzymes. Mitochondrial NAD(P)$^+$-dependent malic enzyme activity and malate-dependent pyruvate formation are progression-linked in Morris hepatomas. *J. Biol. Chem.* **255,** 3844–3848 (1980).
20. Nagel, W. O., Dauchy, R. T. & Sauer, L. A. Mitochondrial malic enzymes. An association between NAD(P)$^+$-dependent malic enzyme and cell renewal in Sprague-Dawley rat tissues. *J. Biol. Chem.* **255,** 3849–3854 (1980).
21. Braig, M. *et al.* Oncogene-induced senescence as an initial barrier in lymphoma development. *Nature* **436,** 660–665 (2005).
22. Chen, Z. *et al.* Crucial role of p53-dependent cellular senescence in suppression of Pten-deficient tumorigenesis. *Nature* **436,** 725–730 (2005).
23. Xue, W. *et al.* Senescence and tumour clearance is triggered by p53 restoration in murine liver carcinomas. *Nature* **445,** 656–660 (2007).
24. Ventura, A. *et al.* Restoration of p53 function leads to tumour regression *in vivo*. *Nature* **445,** 661–665 (2007).
25. Li, T. *et al.* Tumor suppression in the absence of p53-mediated cell-cycle arrest, apoptosis, and senescence. *Cell* **149,** 1269–1283 (2012).

**Supplementary Information** is available in the online version of the paper.

**Acknowledgements** We thank M. J. Birnbaum, B. Vogelstein, W. El-Deiry and M. Lazar for reagents; M. J. Bennett, S. Patel, A. Stonestrom and M. Brewer for technical assistance; and A. Stonestrom for help with manuscript preparation. This work was supported by grants from the National Institutes of Health (CA088868) and the US Department of Defense (W81XWH-10-1-0468) to X.Y.

**Author Contributions** P.J., W.D. and X.Y. designed the study, interpreted the data and wrote the manuscript. P.J. and W.D. performed the experiments. K.E.W. helped with the metabolic studies and data interpretation. A.M. designed the glutaminolytic flux procedure and performed the experiment with the help from P.J.

**Author Information** Reprints and permissions information is available at www.nature.com/reprints. The authors declare no competing financial interests. Readers are welcome to comment on the online version of the paper. Correspondence and requests for materials should be addressed to X.Y. (xyang@mail.med.upenn.edu).

## METHODS

**Antibodies and reagents.** The antibodies against the following proteins/epitopes were purchased from the indicated sources: ME2, actin and β-tubulin (Sigma); AMPK, phospho-AMPK (Thr 172), phospho-p53 (Ser15) and phospho-acetyl-coenzyme A carboxylase (Ser 79) (Cell Signaling Technology); ME1, p21 and PML (Santa Cruz Biotechnology); prohibitin (Thermo Scientific); GAPDH (Novus Biologicals); p53 (DO-1; Oncogene, and Santa Cruz Biotechnology); and MDM2 (Calbiochem, and Santa Cruz Biotechnology). The following reagents were purchased from Sigma: dimethyl L-malate, $NADP^+$, $NAD^+$, doxorubicin, etoposide, trichostatin A, NAC, insulin, troglitazone, dexamethasone and isobutylmethylxanthine.

**Cell culture and gene knockdown with shRNA and siRNA.** Cells were maintained in standard culture conditions without any antibiotic. Expression plasmids for *TP53*, *ME1* and *ME2* shRNA were made in a pLKO.1-puro vector. The targeted sequences for human *TP53* and mouse *Trp53* are 5′-GACTCCAGTGGTAATCTAC-3′ (ref. 26) and 5′-GTACTCTCCTCCCCTCAAT-3′ (ref. 27), respectively. The targeted sequences for human *ME1* and *ME2* are 5′-GGGCATATTGCTTCAGTTC-3′ and 5′-GCACGGCTGAAGAAGCATATA-3′, respectively. Stable shRNA cell lines were established as previously described[28]. siRNAs for *ME1*, *ME2* and *AMPK* were purchased form Invitrogen. siRNA sequences were 5′-AUAACAAUCAGGUAGAAUCUGGUCA-3′ (human *ME1*), 5′-UAUAGUUGAAGGCUUCAGUAUAUUC-3′ (human *ME2*), 5′-CCCUGUGGGUAAAUUGGCUCUAUAU-3′ (human *ME1* no. 2), 5′-CCUGACAAGCCAAUUGACAGAUGAA-3′ (human *ME2* no. 2), 5′-CGUUGAAAAUUGCAGUAAA-3′ (mouse *Me1*), 5′-GGGCACUGAUAACAUGGCACUAUUA-3′ (mouse *Me2*) and 5′-ACCAUGAUUGAUGAUGAAGCCUUAA-3′ (human *AMPK*). siRNAs were transfected into cells using Lipofectamine RNAiMAX Transfection Agent (Invitrogen).

**Semi-quantitative RT–PCR and quantitative RT–PCR.** Total RNA was isolated from cells by TRIzol Reagent (Invitrogen). Two micrograms of RNA for each sample were reversed to complementary DNA by First-strand cDNA Synthesis System (Marligen Biosciences), and 0.2 μg cDNA was used as a template to perform PCR. The primer pairs for human genes were: *ME1*, 5′-ACAGATAATATTTTCCTCACT-3′ and 5′-CTACTGGTCAACTTTGGT-3′; *ME2*, 5′-ATTAGTGACAGTGTTTTCCTA-3′ and 5′-CTATTCTGTTATCACAGG-3′; *p21*, 5′-CCGGCGAGGCCGGGATGAG-3′ and 5′- CTTCCTCTTGGAGAAGATC-3′; *ACTB*, 5′-GACCTGACTGACTACCTCATGAAGAT-3′ and 5′-GTCACACTTCATGATGGAGTTGAAGG-3′; *TP53*, 5′-CACGAGCTGCCCCCAGG-3′ and 5′-TCAGTCGACGTCTGAGT-3′. Primer pairs for mouse genes were: *Me1*, 5′-GATGATAAGGTCTTCCTCACC-3′ and 5′-TTACTGGTTGACTTTGGTCTGT-3′; *Me2*, 5′-TTCTTAGAAG CTGCAAAGGC-3′ and 5′-TCAGTGGGGAAGCTTCTCTT-3′; *p21*, 5′-AACTTCGTCTGGGAGCGC-3′ and 5′-TCAGGGTTTTCTCTTGCAGA-3′; *Actb*, 5′-ACTACATTCAATTCCATC-3′ and 5′-CTAGAAGCACTTGCGGTG-3′; *Trp53*, 5′-GAAGTCCTTTGCCCTGAAC-3′ and 5′-CTAGCAGTTTGGGCTTTCC-3′.

All RT–PCR reactions were performed using the 7900HT Fast Real-Time PCR System (Applied Biosystems) and the amplifications were done using the SYBR Green PCR Master Mix (Applied Biosystems). The thermal cycling conditions were: 50 °C for 2 min followed by an initial de-naturation step at 95 °C for 10 min, 45 cycles at 95 °C for 15 s, 60 °C for 1 min, and a dissociation curve at 95 °C for 15 s and 60 °C for 15 s. The experiments were carried out in triplicate for each data point. Using this method, we obtained the fold changes in gene expression normalized to an internal control gene.

**Cell lysate fractionation and malic enzyme activity.** Cell fractionation was carried out as described[29]. Cells were homogenized in 20 mM HEPES-KOH buffer, pH 7.5, 10 mM KCL, 1.5 mM $MgCl_2$, 1 mM sodium EDTA buffer, 1 mM sodium EGTA buffer and 1 mM dithiothreitol in the presence of 250 mM sucrose and protease inhibitor cocktail (Roche Diagnostics). Homogenates were centrifuged at 500*g* for 5 min at 4 °C, and the supernatant was collected and centrifuged again at 10,000*g* for 20 min to obtain cytosolic and mitochondrial fractions.

ME1 activity was determined using cytosolic extracts as described[30]. The reaction buffer contained 67 mM triethanolamine, 3.3 mM L-malic acid, 0.3 mM β-$NADP^+$ and 5.0 mM manganese chloride. For measuring ME2 activity, mitochondria were purified as described[29] and re-suspended in mitochondrial lysis buffer (20 mM MOPS-KOH, pH 7.4, 250 mM sucrose, 80 mM KCl, 5 mM EDTA, 1 mM PMSF, 1% Triton X-100 and protease inhibitor cocktail) on ice for 30 min by gentle vortexing for 5 s at 5-min intervals. Lysates were centrifuged for 10 min at 14,000 r.p.m. at 4 °C. The enzyme reaction mixtures contained 50 mM Tris-HCl, pH 7.4, 10 mM $MgCl_2$, 0.3 mM $NAD^+$ and 3.3 mM L-malic acid. The reactions were started by adding either cytosolic and mitochondrial extracts, and were monitored by absorbance at 340 nm every 5 s for up to 10 min. Background control was run without L-malic acid as substrate. Enzyme activity was determined by subtracting the activity of the background control to each sample. The resulting changes of absorbance versus time were normalized to protein contents, which were determined using the Bio-Rad protein assay.

**Analysis of malic enzyme gene sequence and chromatin immunoprecipitation (ChIP) assay.** We used the Genomatix Promoter Inspector software (http://www.genomatix.de) to search in malic enzyme genes for potential p53 response elements with the consensus sequence 5′-RRRCWWGYYY-(0–13-base pair spacer)-RRRCWWGYYY-3′, in which R is a purine, Y a pyrimidine, and W either A or T[8]. The sequences for the putative p53 response elements in malic enzyme genes are: ME1-RE, 5′-TTACCTGGTTAACTAGGACTTGCCC-3′; ME2-RE1, 5′-AGGCATGCACCACCATGCCC-3′; ME2-RE2, 5′-AGACCAGTCAAAAACATGTCC-3′; ME2-RE3, 5′-GGGCATGATGGCACATGCCT-3′; and ME3-RE, 5′-TGACTTGGTTTGGCTTTCTTGTCC-3′.

For ChIP assays, cells were washed with PBS and crosslinked with a 1% formaldehyde solution for 15 min at room temperature (25 °C). The crosslinking reaction was stopped by the addition of glycine to 125 mM final concentration. Cell lysates were sonicated to generate DNA fragments with the average size below 1,000 base pairs and followed by immunoprecipitation with indicated antibodies. Bounded DNA fragments were eluted and amplified by PCR. The primer pairs were: ME1-RE, 5′-GCCTTAGTATGTGGATTC-3′ and 5′-GGAAAGCGTAGGGAAGGA-3′; ME2-ME1, 5′-GTTGCCCAGGCTGGAGTG-3′ and 5′-CTGTAATCCCAGCACTTT-3′; ME2-RE2, 5′-TCAGCACTTTGGGAGG-3′ and 5′-GCGACAGAGTCTTGCC-3′; ME2-RE3, 5′-GGCTCAGTGGCTCACG-3′ and 5′-GTGCAGTGGCATG-3′; ME3-RE, 5′-GTTGCGATCCCGTGGCTG-3′ and 5′-ACCGCAGGTCAGACTGAC-3′; p21, 5′-CTGAAAACAGGCAGCCCAAG-3′ and 5′-GTGGCTCTGATTGGCTTTCTG-3′[28].

**Reporter assay.** The DNA fragment containing the potential p53-binding region was amplified by PCR with primers used in the ChIP assay and was cloned into a pGL3-promoter vector (Promega). 293T cells were plated 18 h before transfection in 24-well plates and transiently transfected with 450 ng of the reporter plasmid and/or 100 ng of the p53 plasmid using Lipofectamine 2000 (Invitrogen). The luciferase activity was determined according to the manufacturer's instructions (Promega). Transfection efficiency was normalized on the basis of the Renilla luciferase activity.

**Measurements of metabolites and lipid accumulation.** The levels of NADPH, NADH, $NAD^+$, ATP and ADP in cultured cells were determined using a $NADP^+$/NADPH Quantification Kit, $NAD^+$/NADH Quantification Kit, ATP assay kit, and ADP assay kit (all from BioVision) respectively, following the manufacturer's instructions. Glucose and glutamine consumption was determined using YSI 7100 Multiparameter Bioanalytical System (YSI Life Sciences). Triglyceride was measured using a Triglyceride Assay Kit (BioVision). Total lipids were measured using Oil Red O staining[10]. For this, confluent cells were grown in medium with 10% FBS supplemented with insulin (5 μg $ml^{-1}$), dexamethasone (1 μM), troglitazone (5 μM) and isobutylmethylxanthine (0.5 mM) for 2 days, and in medium supplemented with insulin and rosiglitazone for an additional 5 days. The medium was changed every other day. Cells were then fixed with 4% paraformaldehyde for 30 min at room temperature, washed with distilled $H_2O$ and 60% isopropanol, and stained with a filtered Oil Red O work solution at room temperature. Stain was then removed and cells were washed four times in distilled $H_2O$.

**Measurement of glutaminolytic flux.** Malic-enzyme-dependent glutaminolytic flux was determined by labelling the malate pool with $^{13}C$ from [U-$^{13}C_5$]glutamine and monitoring the conversion of malate to pyruvate indirectly by detecting $^{13}C$-labelled lactate. Carbon-13 enrichments were determined with gas chromatography–mass spectrometry. We observed that this approach results in approximately 50% $^{13}C$ enrichment and allows for the determination of glutaminolytic flux through malic enzyme with high sensitivity. Cells cultured on 10-cm plates with around 60% confluence were transfected with control, *ME1* or *ME2* siRNA. Cells were cultured in regular medium for 60 h and in DMEM containing 12 mM glucose, 3 mM [U-$^{13}C_5$]glutamine and 10% dialysed FBS (Sigma) for an additional 9 h. After medium was removed, cells were immediately quenched with cold 80% methanol. The methanol/cell mass mixtures were centrifuged. The insoluble (protein and lipid) fraction was analysed for protein content. The soluble fraction was dried under a stream of gaseous nitrogen at 40 °C and silylated with *N-tert*-Butyldimethylsilyl-*N*-methyltrifluoroacetamide (MTBSTFA; Regis). The silylated cell extracts were analysed with an Agilent 7890A gas chromatograph/5975C mass spectrometer (Agilent). Mass spectra were quantified with the MSD ChemStation software (Agilent) and corrected for natural abundance contributions from $^{13}C$, $^{29}Si$ and $^{30}Si$ using Isocor (http://www.python.org)[31]. The total lactate level was determined with the YSI 7100 Multiparameter Bioanalytical System. The glutaminolytic flux through malic enzymes was calculated from the equation: $F_{ME} = F_L \times (L_{m+3})/(M_{m+4})$, in which $F_{ME}$ = malic enzyme flux, $F_L$ = total lactate flux, $L_{m+3}$ = fraction of lactate enriched in all three carbons, and $M_{m+4}$ = fraction of malate enriched in all four carbons.

**Measurements of ROS.** ROS levels were determined as described[32]. Cells were incubated at 37 °C for 30 min in PBS containing 10 μM 2',7'-dichlorodihydrofluorescein diacetate (H2-DCFDA, Sigma). Afterwards, the cells were washed twice in PBS, treated with trypsin, and re-suspended in PBS. Fluorescence was immediately measured using a FACScan Flow Cytometer (Becton Dickinson).

**Senescence-associated SA-β-gal activity.** The SA-β-gal activity in cultured cells was determined using a Senescence Detection Kit (BioVision) following the manufacturer's instructions. Percentages of cells that stained positive were calculated by counting 1,000 cells in random fields per cell line.

**Immunofluorescence.** Cells treated with siRNA for 48 h were washed with 1xPBS and fixed in 4% paraformaldehyde. After being treated with 0.1% Triton X-100, cells were stained using anti-PML antibody followed by Texas-red conjugated anti-mouse IgG antibody, and mounted with 4,6-diamidino-2-phenylindole (DAPI) (Vector Laboratories). The images were acquired with a confocal microscope. A total of 200 nuclei were selected randomly and promyelocytic leukaemia nuclear bodies within each nucleus were counted.

**Cell proliferation assay.** Cells were treated with siRNAs for 24 h and seeded in 6-well cell culture dishes in triplicates at a density of 20,000 cells per well in 2 ml of medium containing 10% FBS. The medium was changed everyday. Cells were counted and cell number at the indicated time points was determined.

**Soft agar assay and xenograft tumour models.** For the soft agar assay, cells were suspended in 1 ml of 10% FBS DMEM medium containing a 0.3% agarose and plated on a firm 0.6% agarose base in 6-well plates (5,000 cells per well) as described previously[33]. Cells were then cultured in a 37 °C and 5% $CO_2$ incubator for 2 weeks. Images were obtained and colonies were counted under a microscope. Each experiment was done in triplicate. For the mouse xenograft experiment, cells ($2 \times 10^6$) were injected subcutaneously into the flanks of 4- to 5-week-old athymic Balb-c nu/nu male mice (Taconic Farms). Tumour growth was evaluated at 2 weeks post-injection. All animal experiments were performed in accordance with relevant guidelines and regulations and were approved by the University of Pennsylvania Institutional Animal Care and Use Committee (IACUC).


26. Brummelkamp, T. R., Bernards, R. & Agami, R. A system for stable expression of short interfering RNAs in mammalian cells. *Science* **296,** 550–553 (2002).
27. Ventura, A. *et al.* Cre-lox-regulated conditional RNA interference from transgenes. *Proc. Natl Acad. Sci. USA* **101,** 10380–10385 (2004).
28. Godar, S. *et al.* Growth-inhibitory and tumor-suppressive functions of p53 depend on its repression of *CD44* expression. *Cell* **134,** 62–73 (2008).
29. Jiang, P., Du, W., Heese, K. & Wu, M. The Bad guy cooperates with good cop p53: Bad is transcriptionally up-regulated by p53 and forms a Bad/p53 complex at the mitochondria to induce apoptosis. *Mol. Cell. Biol.* **26,** 9071–9082 (2006).
30. Guay, C., Madiraju, S. R., Aumais, A., Joly, E. & Prentki, M. A role for ATP-citrate lyase, malic enzyme, and pyruvate/citrate cycling in glucose-induced insulin secretion. *J. Biol. Chem.* **282,** 35657–35665 (2007).
31. Millard, P., Letisse, F., Sokol, S. & Portais, J. C. IsoCor: correcting MS data in isotope labeling experiments. *Bioinformatics* **28,** 1294–1296 (2012).
32. Cossarizza, A. *et al.* Simultaneous analysis of reactive oxygen species and reduced glutathione content in living cells by polychromatic flow cytometry. *Nature Protocols* **4,** 1790–1797 (2009).
33. Zhang, J. *et al.* AFAP-110 is overexpressed in prostate cancer and contributes to tumorigenic growth by regulating focal contacts. *J. Clin. Invest.* **117,** 2962–2973 (2007).